

NJC

New Journal of Chemistry

Accepted Manuscript

A journal for new directions in chemistry

This article can be cited before page numbers have been issued, to do this please use: X. Lu, G. Wang, X. Kong, Y. Yu and J. Chen, *New J. Chem.*, 2020, DOI: 10.1039/C9NJ05956C.



This is an Accepted Manuscript, which has been through the Royal Society of Chemistry peer review process and has been accepted for publication.

Accepted Manuscripts are published online shortly after acceptance, before technical editing, formatting and proof reading. Using this free service, authors can make their results available to the community, in citable form, before we publish the edited article. We will replace this Accepted Manuscript with the edited and formatted Advance Article as soon as it is available.

You can find more information about Accepted Manuscripts in the [Information for Authors](#).

Please note that technical editing may introduce minor changes to the text and/or graphics, which may alter content. The journal's standard [Terms & Conditions](#) and the [Ethical guidelines](#) still apply. In no event shall the Royal Society of Chemistry be held responsible for any errors or omissions in this Accepted Manuscript or any consequences arising from the use of any information it contains.

Boron-doped Carbon aerogels supported Cu catalyst for selective hydrogenation of dimethyl oxalate

Xiaodong Lu^{a,b}, Guofu Wang^a, Yu Yang^a, Xiangpeng Kong^c, Jiangang Chen^{*a}

^aState Key Laboratory of Coal Conversion, Institute of Coal Chemistry, Chinese Academy of Sciences, Taiyuan, 030001 Shanxi, PR China

^bUniversity of Chinese Academy of Sciences, Beijing 100049, PR China

^cTaiyuan Institute of Technology, Taiyuan, 030008 shanxi, PR China

Abstract

The Carbon aerogels (CA) was applied to synthesize Cu/CA catalysts by the impregnation method and the catalysts with boron-doped CA supports were systematically characterized and evaluated in the hydrogenation of dimethyl oxalate (DMO). The Cu/xB-CA catalyst with 25wt% copper showed 100% DMO conversion and the highest ethylene glycol(EG) or methyl glycolate(MG) selectivity of 70 % at 230°C, as well a lifetime of over 150h. The characterization results disclosed the reason why the performance of catalysts could be tuned facily by changing the amount of boron doping, which effectively influenced the interrelation between copper and CA, the acidity and alkalinity of catalysts and the Cu dispersion. Both the original carbon aerogels and that promoted with little B could provide larger surface area and high dispersion of metal. The species, size of copper particle and the ratio of Cu⁺/(Cu⁺+Cu⁰) could be regulated by boron doping, thus adjust the type of hydrogenation products.

Keywords:

Carbon aerogels; boron doping; DMO hydrogenation; copper; ethylene glycol; methyl glycolate

1. Introduction

Ethylene glycol (EG) is an important chemical product that has a wide range of applications in the industry, such as the manufacturing of polyester, lubricant, antifreeze additives and solvent^{1,2}. Currently, in industrial production the most common method of synthesizing ethylene glycol is direct hydration of ethylene oxide, which is usually produced from petroleum-derived ethylene. Due to the shrinking of crude oil resources, the conventional ethylene oxidative hydrolysis process, which relies on the petrochemical industry to synthesize ethylene glycol, confront enormous challenges³. Owing to the reduction of crude oil resources as well the increase in demand for ethylene glycol, the synthesis of ethylene glycol from coal has attracted a lot of interests and commercialized in China to reduce the dependence on petroleum resource⁴⁻⁷. Methyl glycolate (MG) is an important platform material and chemical intermediate, and has been widely used in the synthesis of value-added products in the pharmaceutical, fine chemical, and perfume industries¹. At present, several methods for synthesizing MG have been developed, such as carbonylation of formaldehyde with carbon monoxide, coupling of methyl formate with formaldehyde under strong acid

1
2
3 catalysis, and high pressure esterification¹⁻³. The main disadvantages of these processes are limited source of raw materials
4 harsh reaction conditions, complex separation techniques, severe reactor corrosion, and low yields of target products⁴⁻⁷. Now, View Article Online
5 the new route of synthesizing EG/MG under mild conditions with cheap syngas as raw material has become a research highlight, <https://doi.org/10.1039/C9NJ05956C>
6 mainly including two steps: coupling carbon monoxide with nitrite ester to synthesize dimethyl oxalate (DMO), then catalytic
7 hydrogenation of DMO to EG/MG^{3, 8}. Although the silica supported copper catalysts have been extensively investigated for
8 hydrogenation of DMO as a result of their high catalytic activity for DMO hydrogenation⁹, the usage of silica support could be a
9 fatal flaw in the DMO hydrogenation process because of the leaching of the silica under the gas phase reaction condition
10 containing methanol¹⁰. The development of other support material is important for obtaining highly active and stable Cu-based
11 catalyst for DMO hydrogenation from commercial application prospect. Noritatsu Tsubaki¹¹ et al. Reported that boron doped
12 carbon nanotubes was used as the support of copper based catalyst for DMO hydrogenation to ethanol, and the ethanol
13 selectivity was 78% (300 °C, 2.5 MPa, H₂/DMO = 200). Ren¹² et al. Reported that the activated carbon aerogel supported copper
14 catalyst was applied to the hydrogenation of DMO to ethanol, and its selectivity of ethanol was 62% (2.0 MPa, 330 °C, H₂/DMO
15 = 60). Carbon aerogels are widely used in catalyst supports, capacitors, fuel cells, adsorber/separator and other fields because of
16 their superior porosity, high specific surface area, low density and excellent electrochemical performance¹³⁻¹⁷. Therefore, the
17 boron-doped Carbon aerogels was adopted as a support for Cu catalyst to carry out the DMO hydrogenation. By doping
18 different proportion of boron to CA, the interaction between copper and support and the species of rare copper were also
19 affected, thus different hydrogenation products(EG/MG) were obtained. All along, the types of DMO hydrogenated products are
20 mainly controlled by temperature. We found that the addition of different amounts of boron in the carbon aerogel could achieve
21 the hydrogenation product deployment, which reduced energy consumption in industry. In this work, various Cu/xB-CA
22 catalysts were prepared by thermal treating CA in the presence of boric acid followed by impregnation with Cu species, and
23 their catalytic performances were evaluated in the hydrogenation of DMO. On basis of systematic characterizations, the effect of
24 boron doping on the size of copper nanoparticles, interaction between Cu species and CA support, Cu⁰ and Cu⁺ distribution,
25 along with surface acidity of Cu/CA catalysts were elucidated. Thus, the catalytic performance could be controlled and
26 hydrogenation products were modulated. Our results may encourage readers to design and investigate other related carbon
27 materialbased catalysts with favorable performances for the hydrogenation of DMO.

2. Experiment

2.1. Catalyst preparation

40
41
42
43
44
45 Carbon aerogels: Resorcinol and formaldehyde (molar ratio) were mixed in a ratio of 1:2. Sodium carbonate was added as
46 catalyst and stirred in inert gas atmosphere for 30 minutes. Subsequently, refined constant temperature for 7 days, followed by
47 acidification with 3% acetic acid for 1 day, then replacement with tert-butanol for 3 days, freeze-drying. After 800 °C (ramping
48 rate: 5 °C/min) hours of carbonization in a high temperature tubular furnace for three hours, carbon aerogels were obtained¹⁸.

49
50
51
52
53
54
55
56
57
58
59
60
xB-CA supports: the boron-doped CA supports were prepared by thermal annealing of a mixture of CA and boric acid. CA and
boric acid were mixed with different weight ratio (boric acid: CA = 0.1: 1, 0.3:1, 0.5:1, 1: 1, respectively) and the uniform
mixture were obtained by grinding for about 30 minutes. Then, the mixture was calcined at 1000 °C for 4 hours in argon
atmosphere and cooled to room temperature. Finally, the collected sample was washed with deionized water before drying at
90 °C in vacuum. The corresponding supports were denoted as 0.1B-CA, 0.3B-CA, 0.5B-CA, 1B-CA, respectively.

Cu/xB-CA catalysts: Cu/xB-CA catalysts were prepared by sonication-assisted impregnation method, in which the loading of Cu
was 25 wt%. Quantitative Cu(NO₃)₂•3H₂O was dissolved in deionized water, then dripped into xB-CA supports, and stirred for
30 minutes before ultrasonic treatment. All of these operations were carried out at room temperature. The resulting solid was

dried for 12h at 90°C in vacuum and then calcined at 500 °C (ramping rate: 3°C/min) under argon atmosphere for 3h. Cu/Ca catalyst preparation method was the same as above.

View Article Online
DOI: 10.1039/C9NJ05956C

2.2. Catalyst test

Catalytic test of DMO hydrogenation was conducted in a continuous flow mode using a fixed bed reactor. Calcined catalyst mixed with quartz sand was placed in the middle of the reactor, and quartz wool was filled on both sides of the catalyst bed. Then, the system was heated to reduction temperature (300°C), and the system pressure was precisely controlled at 2.4 MPa, and the reaction temperature is 230°C. Then, a 30 wt% DMO solution with methanol as solvent was continuously pumped into the reactor with co-feeding H₂ at a H₂/DMO molar ratio of 180. Finally, the products were condensed in a cold trap and analyzed by using a gas chromatography instrument equipped.

2.3. Catalyst characterization

Copper loading was determined by inductively coupled plasma emission spectroscopy (ICP-OES). The Brunauer–Emmett–Teller (BET) surface area (S_{BET}), pore volume (V_p) were tested via N₂ physical adsorption at -196°C. All samples were degassed under vacuum at 90°C for 1 h before measurement and then degassed at 350°C for 8 h. The metallic Cu surface area and copper dispersion was the adsorption and decomposition of N₂O with the pulse titration method. The acidic strength of the catalyst surface was titrated by NH₃-TPD. The calcined catalyst of 30 mg was degassed at 350°C for 1 h under Ar. Then the temperature was cooled to room temperature and NH₃ was adsorbed (30ml/min, 0.5h). Finally, the desorption signal of NH₃ was recorded by mass spectrometry after blowing with Ar for 1 h, then rising to 600°C with 15°C/min. The defect level in catalysts was evaluated by Raman spectra, and the experiments that the excitation wavelength was 532nm and power was 12mW were operated on a HORIBA evolution equipment at room temperature. X-ray diffraction (XRD) was carried out with a D/max-RA X-ray diffractometer, and the patterns were acquired from 5°C to 85°C with a rate of 10°C/min. For the reduced samples, catalysts were reduced at 300°C for 4 h, then cooled to room temperature and sealed in a centrifuge tube to avoid oxidation. Temperature-programmed reduction (TPR) was conducted in an atmospheric quartz reactor (5 mm i.d.). The calcined catalyst of 25 mg was gasified for 1 h at 100°C under Ar. After cooling to room temperature under Ar, the gas was switched to 5% H₂/Ar, and the sample was heated to 800°C at a heating rate of 10°C/min. Thermal conductivity detector (TCD) was used to monitor the consumption of H₂. Copper on the surface of reduction catalyst was determined by X-ray photoelectron spectroscopy (XPS) and Auger electron spectroscopy (XAES) at Perkin Elmer Phi 1600 ESCA.

3. Results and discussion

3.1. Properties of Cu/xB-CA

Table 1. Physicochemical properties of Cu/CA and Cu/xB-CA catalysts.

Catalyst	Cu loading (wt%) ^[a]	S _{BET} (m ² /g) ^[b]	V _p (cm ³ /g) ^[b]	d _{Cu0} (nm) ^[c]	S _{Cu} (m ² /g) ^[c]	D _{Cu} (%) ^[c]	S _{Cu⁺} (m ² /g) ^[d]	Cu ⁺ /(Cu ⁰ +Cu ⁺) (%) ^[e]	acid amount (mmol/g cat) ^[f]
Cu/CA	25.1	399.03	0.22	2.4	72.1	42.6	32.9	31.3	0.019
Cu/0.1B-CA	24.9	299.36	0.19	2.3	73.6	43.5	43.8	37.3	0.037
Cu/0.3B-CA	25.5	284.20	0.16	4.1	40.9	24.2	35.1	46.2	0.028
Cu/0.5B-CA	25.7	9.69	0.02	7.7	22.0	13.0	20.1	47.7	0.021
Cu/1.0B-CA	25.3	6.51	0.01	10.2	16.6	9.5	21.0	55.9	0.023

[a] Cu loading determined by ICP-OES analysis. [b] Determined by N₂ isotherm adsorption. [c] Determined by the N₂O titration method. [d] Calculated S_{Cu⁺} by N₂O titration and Cu LMM XAES spectra. [e] Peak area ratio between Cu⁺ and (Cu⁺+Cu⁰) by deconvolution of Cu LMM XAES spectra. [f] Amount of acid sites estimated by NH₃-TPD.

The copper loading of calcined Cu/xB-CA catalysts were detected by ICP-OES and summarized in Table 1. The Cu amount of those catalysts were similar. The texture characteristics and the dispersion of copper was also listed in Table 1. The BET surface area values and the pore volume of Cu/xB-CA catalysts varied upon the boron doping. With the increment of boron doping ratio from 0 to 1, the BET surface area decreased from 399 m²/g to 6.51 m²/g. Meanwhile, the pore volume decreased from 0.22 cm³/g to 0.01 cm³/g. The decrease of BET surface area may be attributed to that collapse of porous carbon matrix as more B substituted carbon atoms. N₂ adsorption-desorption isotherms of calcined Cu/xB-CA catalysts were shown in Figure 1. All the N₂ adsorption-desorption isotherms of Cu/xB-CA presented typical type IV Langmuir isotherms with a H4-type hysteresis loops, indicating that the pore were mainly composed of mesoporous and microporous one. The XPS characterization was implemented to confirm the presence of the doped boron. The XPS survey spectra of Cu/CA and Cu/xB-CA were illustrated in Figure 2. For Cu/CA, no B1s peak was detected due to the absence of boron source. In addition to the C1s peak, a small B 1s peak was detected in the spectrum of xB-CA, which proved the successful doping of boron. The use of Raman spectra as a method for the characterization of graphite was first reported by Tuinstra¹⁹. Those catalyst were subjected to Raman characterization and shown in Figure 3, The band near 1350 cm⁻¹ (d-band) is associated with disorder induced scattering due to defects in the carbon structure or loss of hexagonal symmetry^{20, 21}. In Figure 3, as the doping amount of boron increases, the D band shifted to the left and the G band did not shift substantially which indicated that the addition of boron can enhance the carbon aerogel structure to be more ordered. The NH₃-TPD measurement was taken to evaluate the strength and quantity of acidic sites on Cu/xB-CA catalysts and the obtained profiles were compared in Figure 5 and Table 1. The acidity of the catalyst and its contribution were not entirely dependent on boron. The addition of boron first increased the acidity to a certain extent, and then the acidity decreased as the boron content increases furthermore. Boron doping could improve the acidity of catalyst, because boron played the role of electron acceptor Lewis acid in catalyst. As shown in Figure 6, it could be clearly seen that the amount of boron doping was different, the existence form of the metal in the catalyst was different, and its acidity was also different. Cu/0.1B-CA catalyst had the strongest acidity because of the contribution of boron and the existence of Cu²⁺ on its surface, which had a stronger ability to accept electrons. For DMO hydrogenation, the metallic Cu catalyzes the conversion of C=O bonds and C-O bonds in DMO to MG and EG step-by-step with the assistance of acid sites in activating these bonds²². Therefore, when the acidity was strong (Fig. 4 (b)), this was conducive to the conversion of DMO and the formation of EG. To clarify the morphology of the Cu/CA and Cu/xB-CA catalysts, the TEM image of the calcined catalysts was shown in Figure 4. With the increase of boron doping ratio, it can be seen that the copper particles tend to form regular patterns. The Cu particle size became smaller upon B modification, then increased monotonously with B amount, which was consistent with the results of Table 1. It can also be seen that the support structure of the catalyst would be destroyed with excessive boron doping, and the

support structure would change from amorphous matrix to sheet-like one, which was consistent with the variation of specific surface area in Table 1. The N_2O titration was taken to evaluate the particle size, dispersion and Cu exposed surface area. As shown in Table 1, the dispersion of copper nanoparticles followed the order of $Cu/0.1B-CA > Cu/CA > Cu/0.3B-CA > Cu/0.5B-CA > Cu/1B-CA$, and the TEM images also displayed the similar result. As shown in Table 1, both the Cu^0 surface area and Cu^+ surface area increased then decreased with increased boron content. This phenomenon could be attributed to the following reasons: 1) The dispersion of supported Cu species could be improved by boron doping into the CA, resulted in large Cu exposed surface area. However, when boron was excessive, the structure of CA would be destroyed and the surface of Cu^0 was decreased. 2) the doped boron could interact strongly with positive-valence Cu species, keeping highly dispersed Cu^+ sites simultaneously. The surface area of Cu^+ decreased when the structure was destroyed.

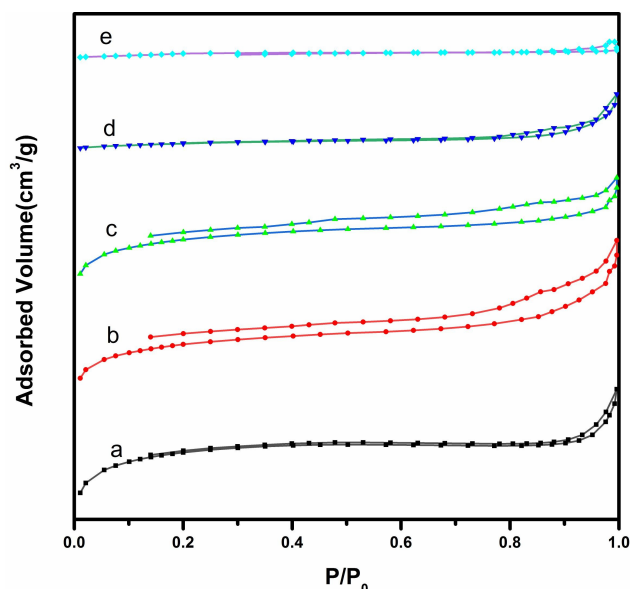


Figure 1. Adsorption isotherms of catalyst: (a) Cu/CA, (b) Cu/0.1B-CA, (c) Cu/0.3B-CA, (d) Cu/0.5B-CA, (e) Cu/1B-CA.

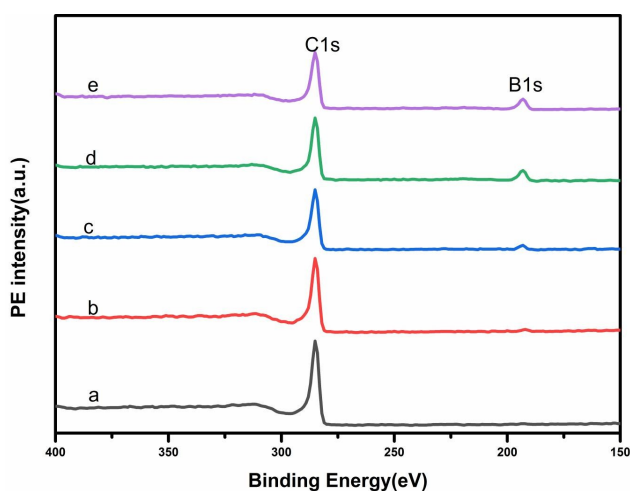
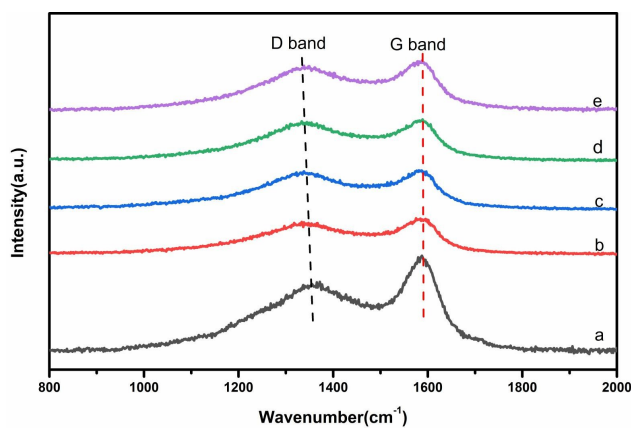


Figure 2. XPS part of survey spectra of catalyst: (a) Cu/CA, (b) Cu/0.1B-CA, (c) Cu/0.3B-CA, (d) Cu/0.5B-CA, (e) Cu/1B-CA.



View Article Online
DOI: 10.1039/C9NJ05956C

Figure 3. Raman spectra of survey spectra of catalyst: (a) Cu/CA, (b) Cu/0.1B-CA, (c) Cu/0.3B-CA, (d) Cu/0.5B-CA, (e) Cu/1B-CA.

1
2
3
4
5
6
7
8
9
10
11
12
13
14
15
16
17
18
19
20
21
22
23
24
25
26
27
28
29
30
31
32
33
34
35
36
37
38
39
40
41
42
43
44
45
46
47
48
49
50
51
52
53
54
55
56
57
58
59
60

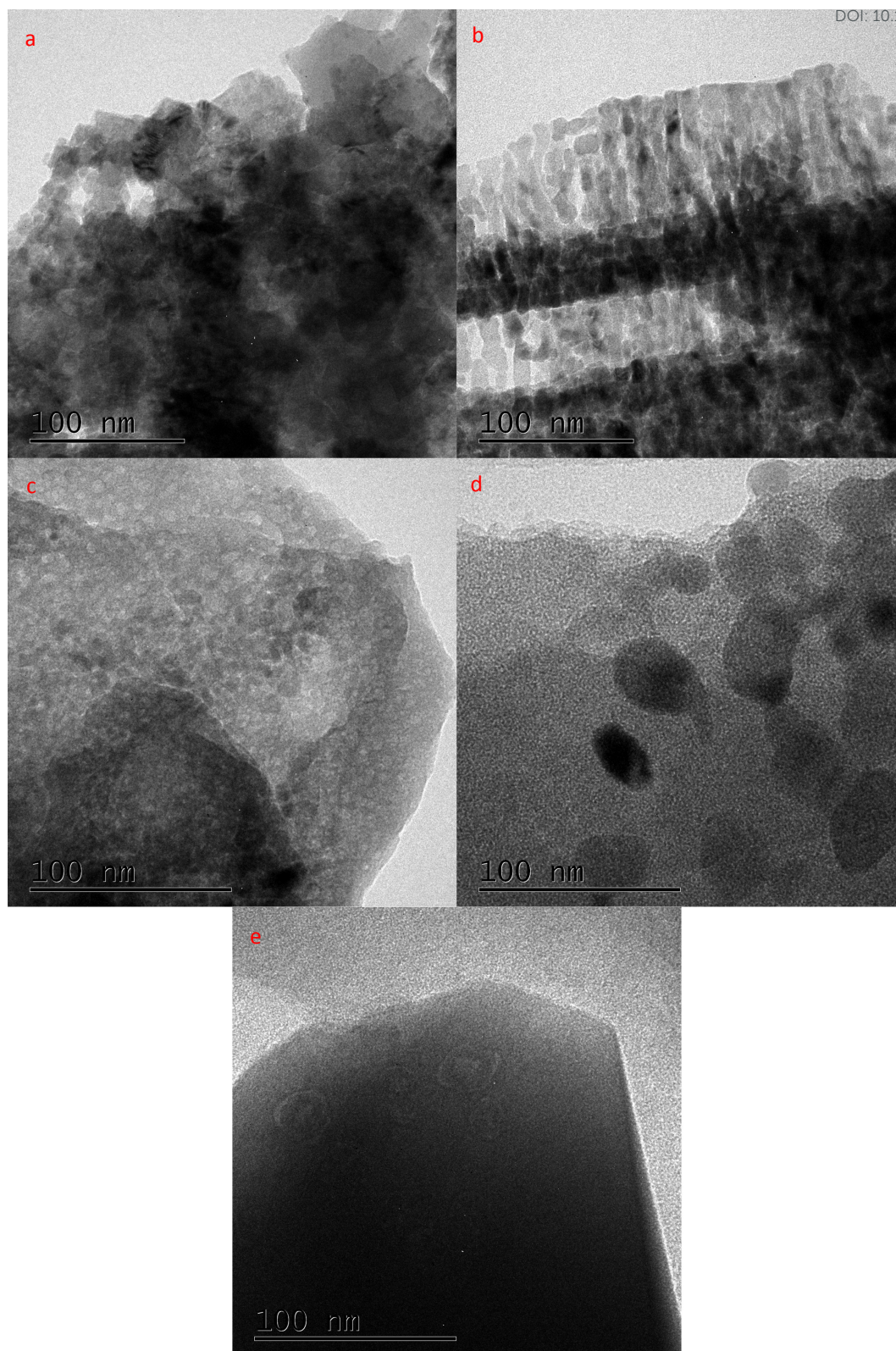
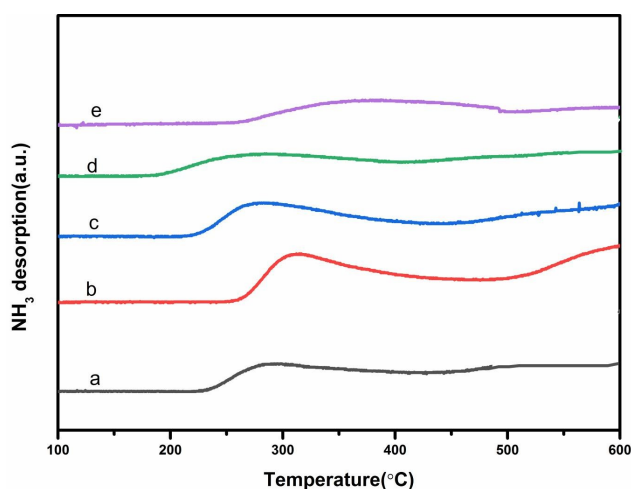


Figure 4. TEM images of calcined catalysts: (a) Cu/CA, (b) Cu/0.1B-CA, (c) Cu/0.3B-CA, (d) Cu/0.5B-CA, (e) Cu/1B-CA.



View Article Online
DOI: 10.1039/C9NJ05956C

Figure 5. NH_3 -TPD of calcined catalyst: (a) Cu/CA, (b) Cu/0.1B-CA, (c) Cu/0.3B-CA, (d) Cu/0.5B-CA, (e) Cu/1B-CA.

3.2. XRD profiles

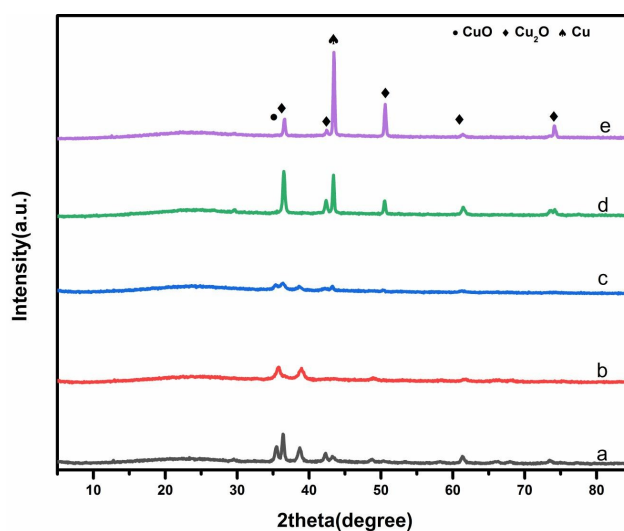


Figure 6. XRD patterns of calcined catalyst: (a) Cu/CA, (b) Cu/0.1B-CA, (c) Cu/0.3B-CA, (d) Cu/0.5B-CA, (e) Cu/1B-CA.

X-ray diffraction patterns of calcined Cu/xB-CA catalysts are shown in Figure 6. The Cu_2O and metallic Cu peaks indicated that the facile reduction of copper species by CA support took place even in the absence of hydrogen^{23, 24}. Compared with Fig. 6 (b) and (c), when the amount of boron added was relatively small, the peaks of CuO (2theta = 35.4 and 38.6(JCPDS05-0661)) of (b) and (c) were more obvious than that of a, probably because the boron doping in CA enhanced the interaction between Cu^{2+} and CA. With increasing amount of doped boron, the peak of Cu_2O (JCPDS05-0667) appeared first, then decreased, and the peak of Cu (JCPDS04-0836) increases continuously. This indicated that the addition of boron could hinder the further transformation from Cu^{2+} to Cu^+ and Cu^0 . However, as the amount of boron was increased excessively (Figure 6 (d) (e) (f)), it would promote the transformation of Cu^+ to Cu. Therefore, from XRD results, it is reasonable to conclude that boron doping could affect the reduction of Cu species. The influence of boron doping on the interaction of Cu species with CA support could be further investigated by H_2 -TPR as shown in Figure 8.

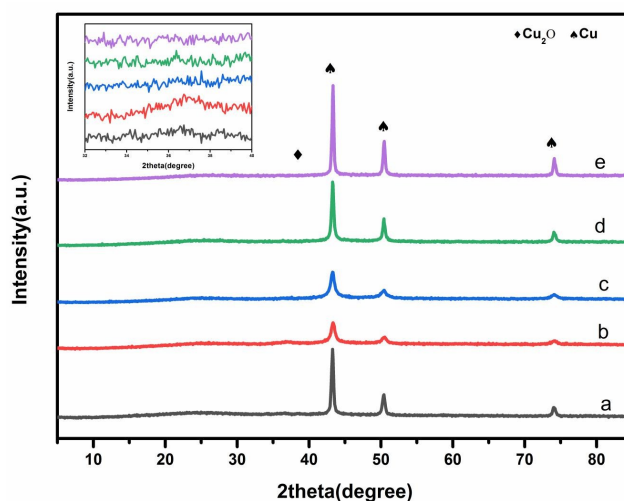


Figure 7. XRD patterns and part of XRD patterns of reduced catalyst: (a) Cu/CA, (b) Cu/0.1B-CA, (c) Cu/0.3B-CA, (d) Cu/0.5B-CA, (e) Cu/1B-CA.

X-ray diffraction patterns of reduced Cu/xB-CA catalysts are shown in Figure 7. After hydrogen reduction, Cu^{2+} are transformed into Cu^0 . However, due to the appropriate amount of boron doping, the degree of crystallization and particle size of Cu^0 were changed. This may be due to the addition of appropriate boron, the relationship between Cu^0 and CA was strengthened, and the growth of copper nanoparticles is limited, but when the amount of boron increases, the limiting effect will be weakened. There was a distinct asymmetric peak in Figure 10, indicating the presence of Cu_2O , but there was no significant Cu_2O peak in Figure 7. This was due to that the Cu_2O particles were too small and were present only on the surface of the catalyst, resulting in poor crystallization.

3.3. TPR profiles

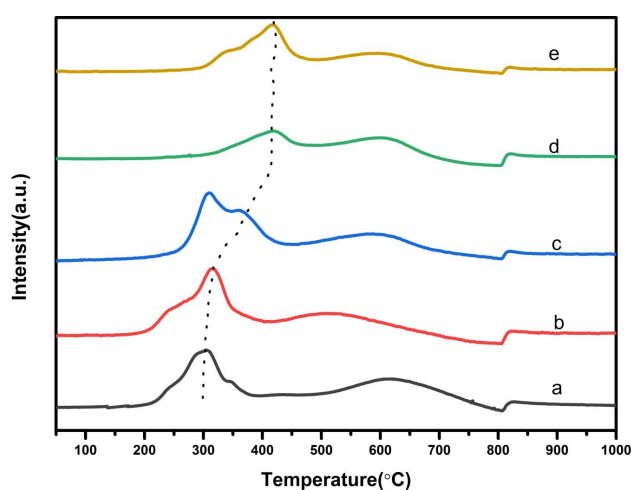


Figure 8. TPR patterns of calcined catalyst: (a) Cu/CA, (b) Cu/0.1B-CA, (c) Cu/0.3B-CA, (d) Cu/0.5B-CA, (e) Cu/1B-CA.

The TPR measurements (Figure 8) were performed to investigate the interaction between Cu species and CA support and reducibility of Cu/xB-CA catalysts with different amount of boron. The Cu/xB-CA catalysts with boron doping showed much higher reduction temperature and the reduction peak gradually shifted to higher temperature with increased boron amount. As an

electron-deficient element, boron doped in the graphitic structure of CA could strengthen the interaction of positive-valence Cu species with CA support²⁵. Therefore, boron doping hindered the transformation of the positive-valence Cu species to metallic Cu to some extent¹¹. However, when the ratio of boron to CA exceeds 0.5:1, the reduction temperature remains basically unchanged, which may be due to the limited amount of boron entering CA support and the limited interaction between Cu and CA support. When the ratio of boron to CA is less than 0.3:1, the small shoulder peak may be caused by different copper species²⁶. When the ratio is greater than 0.5:1, the small shoulder peak may be affected by different Cu⁺ states. In addition, due to the reduction of hydrogen at high temperature, the oxygen-containing functional groups on the surface of CA support are gasified, resulting in the peak of hydrogen consumption at about 600°C^{27,28}.

3.4. XPS

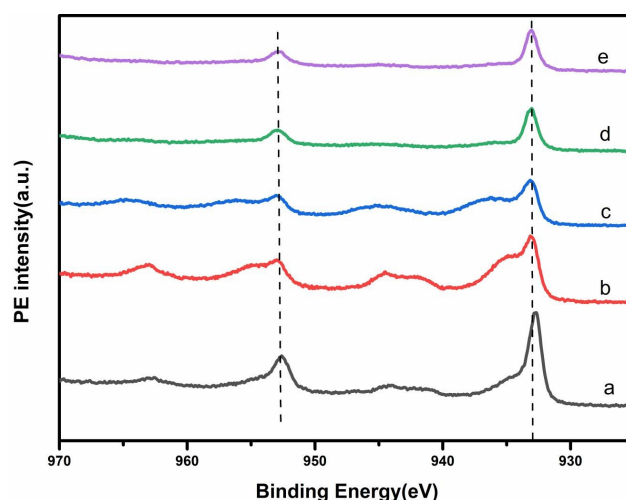
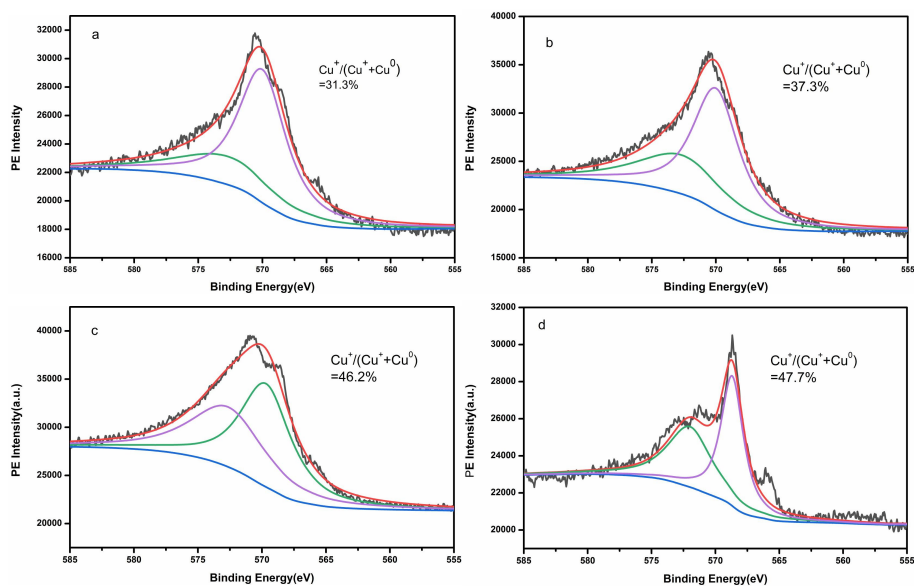


Figure 9. XPS patterns of calcined catalyst: (a) Cu/CA, (b) Cu/0.1B-CA, (c) Cu/0.3B-CA, (d) Cu/0.5B-CA, (e) Cu/1B-CA.



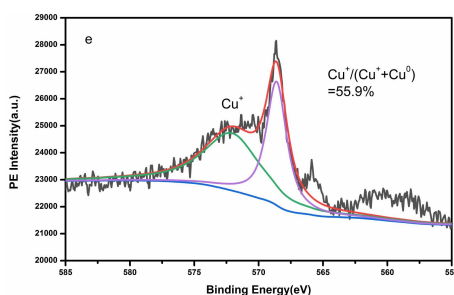
View Article Online
DOI: 10.1039/C9NJ05956C

Figure 10. Cu LMM Auger spectra of reduced Cu/xB-CA catalysts: (a) Cu/CA, (b) Cu/0.1B-CA, (c) Cu/0.3B-CA, (d) Cu/0.5B-CA, (e) Cu/1B-CA.

The surface chemistry of the Cu/xB-CA and reduced Cu/xB-CA catalyst was detected by XPS and X-ray induced Auger spectroscopy (XAES) measurements. As shown in Figure 9, the intensive photoelectron peaks of samples at 933.1 eV and 952.8 eV were assigned to the binding energy (BE) of Cu 2p_{3/2} and Cu 2p_{1/2}, respectively²⁹. Meanwhile, there were some peaks (Fig 8 a b c) between 942 and 944 eV, which be ascribed to Cu⁺ implying incomplete reduction of Cu²⁺ to Cu⁰. This phenomenon corresponds to the XRD spectrum (a b c). As shown in Figure 10, all the Cu LMM spectra of reduced catalysts presented an asymmetrical and broad peak, suggesting the stable coexistence of Cu⁺ and Cu⁰ on the surface of these catalysts. The concentration of Cu⁺ and Cu⁰ on the surface can be determined by the ratio between their band intensities in the Cu LMM XAES spectra^{30, 31}. The distributions of Cu⁺ and Cu⁰ species showed distinct changes with the boron doping³². The ratio of Cu⁺/(Cu⁺+Cu⁰) of (a) Cu/CA, (b) Cu/0.1B-CA, (c) Cu/0.3B-CA, (d) Cu/0.5B-CA and (e) Cu/1B-CA were 31.3%, 37.3%, 46.2%, 47.7% and 55.9%, respectively. The ratio of Cu⁺/(Cu⁺+Cu⁰) increases as the boron content increases, which also indicates that boron doping hinder the reduction of copper species. Comparing with Figure 7, the presence of asymmetric peaks indicates the coexistence of Cu⁺ and Cu⁰, while there were only obvious peaks of Cu⁰ in Figure 7, probably due to the better dispersion of Cu on the catalyst surface and poor crystallinity.

3.5. Catalytic performance

The catalytic performance of Cu/xB-CA catalyst prepared by impregnation method was studied in a fixed-bed reactor by DMO gas-phase hydrogenation. The reaction was carried out at the temperature of 230 °C, the total system pressure was maintained at 2.4 MPa and the molar ratio of H₂/DMO was 180. The LHSV of DMO was 1h⁻¹. It is know that the hydrogenation reaction of DMO involves several steps of reactions:

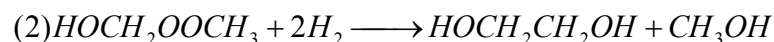
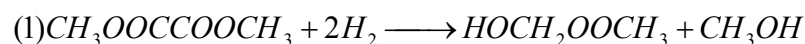


Table 2. DMO hydrogenation to EG over Cu/CA and Cu/xB-CA catalysts.

View Article Online
DOI: 10.1039/C9NJ05956C

Catalyst ^[a]	T(°C)	CONV _(60h) ^[c] (%)	SEL _(60h) (%) ^{[b][c]}				CONV _(130h) ^[d] (%)	SEL _(130h) (%) ^{[b][d]}			
			EG	MG	Ethanol	Other		EG	MG	Ethanol	Other
Cu/CA	230	100.0	71.0	13.0	1.4	14.6	100.0	60.2	22.9	4.4	12.5
Cu/0.1B-CA	230	100.0	68.4	14.8	5.2	11.2	96.4	67.4	21.6	2.8	8.2
Cu/0.3B-CA	230	84.6	45.2	37.3	1.3	16.2	48.9	30.2	50.0	3.1	16.7
Cu/0.5B-CA	230	73.8	41.7	37.2	3.0	18.1	42.2	17.4	50.7	3.0	28.9
Cu/1.0B-CA	230	73.4	9.4	65.9	3.3	21.4	64.9	11.2	55.4	2.1	31.3

[a] Reaction conditions: 230 °C, 2.4 MPa, LHSV = 1 h⁻¹, H₂/DMO=180, reaction time=12h, 30wt% DMO/methanol as feed. [b] MG: methyl glycolate, EG: ethylene glycol, Others mainly consist of H₂O, methyl methoxyacetate, methyl acetate. [c] 60h: the reaction time was 60 hours. [d] 130h: the reaction time was 130 hours.

The DMO hydrogenation reaction catalyzed by boron-free and boron-doped catalysts was executed under the same reaction conditions, which study the effect of boron doping on the catalytic performance. The conversion of DMO and selectivity of product were listed in Table 2(detailed data are shown in Table S1 S2 and S3). The conversion of DMO and the selectivity of EG and MG showed significant regular changes.

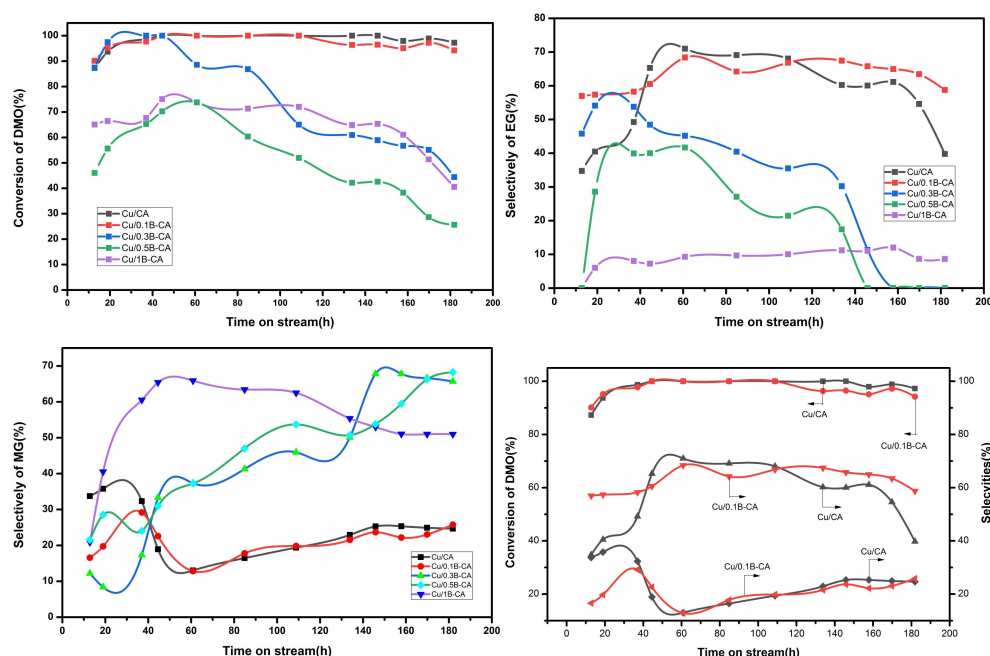


Figure 11. Spectra of Catalytic activity

Reaction conditions: 300 °C, 2.4 MPa, LHSV = 1 h⁻¹, H₂/DMO = 180, 30wt% DMO/methanol as feed.

The DMO conversion of Cu/CA and Cu/0.1B-CA was close to 100%, while the other catalysts are low initially and are rising along the time on stream. After about 50 h, there was a downward trend. An optimum EG selectivity of about 70% was obtained on Cu/CA and Cu/0.1B-CA catalysts. Combining with the characterization results, the Cu/CA catalyst with the best activity showed the highest specific surface area (as shown in Table 1). For instance, the specific surface area of the catalyst followed the order of Cu/CA > Cu/0.1B-CA > Cu/0.3B-CA > Cu/0.5B-CA > Cu/1B-CA, which is in accordance with activity sequence. The DMO conversion of Cu/0.3B-CA, Cu/0.5B-CA and Cu/1B-CA catalysts was relatively low, mainly due to the excessive boron addition, which caused the structure of the catalyst to be destroyed to varying degrees (as shown in Table 1). With regards

to the size of copper nanoparticles and $\text{Cu}^+ / (\text{Cu}^0 + \text{Cu}^+)$, they are correlated with the selectivity of the catalyst. As shown in Table 1, the dispersion of copper nanoparticles followed the order of $\text{Cu}/0.1\text{B-CA} > \text{Cu}/\text{CA} > \text{Cu}/0.3\text{B-CA} > \text{Cu}/0.5\text{B-CA} > \text{Cu}/1\text{B-CA}$, which comply with the EG selectivity order. Compared with EG, the selectivity of MG of $\text{Cu}/0.3\text{B-CA}$, $\text{Cu}/0.5\text{B-CA}$ and $\text{Cu}/1\text{B-CA}$ catalysts was higher, which was related to the interaction between Cu and CA after mass boron addition (as shown in Figure 7), thus the specific surface area and ratio of Cu^+ and Cu^0 changed dramatically (as shown in Table 1), thereby the progress of reaction 2 was suppressed. That is to say, when the ratio of $\text{Cu}^+ / (\text{Cu}^+ + \text{Cu}^0)$ reached a suitable value, the dispersion of copper was optimized, the selectivity of EG reached maximum value and the catalyst became more stable. Cu^0 activates H_2 and Cu^+ adsorbs carbonyl groups, the reaction proceed smoothly according to the supposed reaction mechanism³³. As can be seen from Table 1, only when Cu^0 and Cu^+ cooperate, can EG selectivity be maximized. When the amount of Cu^0 was small, less hydrogen was activated in comparison with activated carbonyl, so that reaction 2 was restricted, thus produced more MG.

Fig. 11 also shown the stability of $\text{Cu}/0.1\text{B-CA}$ catalyst in comparison with that of Cu/CA catalyst. The $\text{Cu}/0.1\text{B-CA}$ catalyst was more stable after 120h. The improved stability was attributed to the enhanced interaction between Cu species and CA support by the doped boron, which might reduce the sintering of Cu to some extent. However, the amount of boron should not be too much, otherwise the structure of catalyst will be destroyed (see Table 1), and the stability of catalyst would be reduced.

4. Discussion

As shown in Table 2, $\text{Cu}/0.1\text{B-CA}$ catalyst shows the best catalytic activity in DMO hydrogenation. Generally speaking, the catalytic performance of copper catalyst was related to the dispersion of copper and the $(\text{Cu}^+ + \text{Cu}^0)$ ratio of copper³⁴. In this work, carbon aerogels with abundant micropores and high specific surface areas were obtained. The highest BET specific surface area was $399\text{m}^2/\text{g}$, which made the dispersion of copper nanoparticles very high, thus further improved the catalytic performance. In addition, as the anchor point, the occurrence of micropores in the carrier greatly enhanced the dispersion of copper particles³⁵, which was verified by TEM analysis (Fig. 4) and N_2O titration (Table 1). It had been reported that the synergistic effect of Cu^0 and Cu^+ was very important for the catalytic activity of ester hydrogenation^{36, 37}. As shown in Table 1 and table 2, the activity of Cu catalyst increases with the increase of Cu^0 content. In $\text{Cu}/0.1\text{B-CA}$, the highest DMO conversion and EG selectivity were achieved when the ratio of $\text{Cu}^+ / (\text{Cu}^+ + \text{Cu}^0)$ was 37.3%. The analysis is as follows: only when Cu^0 and Cu^+ cooperate, can EG selectivity be maximized. When the amount of Cu^0 was small, less hydrogen was activated in comparison with activated carbonyl, so that reaction 2 was restricted, thus produced more MG.

5. Conclusion

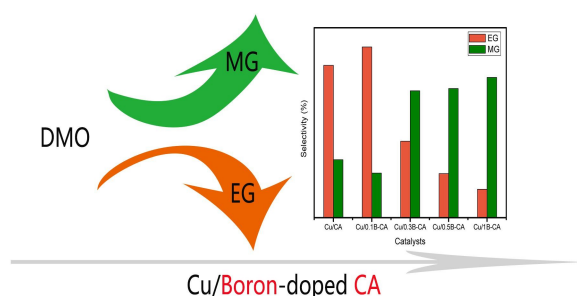
In summary, the doping of boron to CA support will change the Cu catalysts structure greatly as well as the performance in DMO hydrogenation. The pore size has little change, but the specific surface area change obviously. The Cu^+ and Cu^0 specific surface area increased upon B addition, then decreased monotonously with more B content. Both the Cu dispersion and acidity maximized at $\text{Cu}/0.1\text{B-CA}$ catalyst. Acid-base and the interaction of copper with CA are changed by boron doping, so that the copper particle size of the catalyst, Cu dispersion and the ratio of $\text{Cu}^+ / (\text{Cu}^+ + \text{Cu}^0)$ were changed. The $\text{Cu}/0.1\text{B-CA}$ catalyst exhibited superior catalytic performance in the hydrogenation of DMO to EG, achieved the highest EG selectivity and DMO

conversion, which could be attributed to small copper particle size, high copper dispersion, matchable interaction strength between suitable Cu substances and CA support, appropriate Cu⁰ and Cu⁺ distribution and suitable surface acidity. Therefore, boron doping is an effective method to improve the catalytic performance of CA-based catalysts and to guide the direction of hydrogenation scheme for DMO hydrogenation.

Acknowledgement

This work was supported by the Chinese Academy of Sciences Strategic Pilot Science and Technology Special (Class A) (XDA21020000), the National Natural Science Foundation of China (21673272), the autonomous research project of State Key Laboratory of Coal Conversion (SKLCC 2018BWZ001).

Graphical Abstract



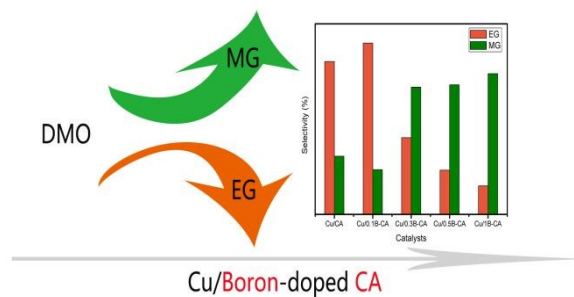
The modification of B in carbon support can modulate the hydrogenation selectivity.

References

1. G. H. Xu, Y. C. Li, Z. H. Li and H. J. Wang, *Industrial & Engineering Chemistry Research*, 1995, **34**, 2371-2378.
2. H. Yue, Y. Zhao, X. Ma and J. Gong, *Cheminform*, 2012, **41**, 4218-4244.
3. L. Chen, P. Guo, M. Qiao, S. Yan, H. Li, S. Wei, H. Xu and K. Fan, *Journal of Catalysis*, 2008, **257**, 172-180.
4. F. E. Celik, H. Lawrence and A. T. Bell, *Journal of Molecular Catalysis A Chemical*, 2008, **288**, 87-96.
5. H. Liu, Z. Huang, C. Xia, Y. Jia, J. Chen and H. Liu, *Chemcatchem*, 2015, **6**, 2918-2928.
6. J. Pang, M. Zheng, A. Wang and T. Zhang, *Industrial & Engineering Chemistry Research*, 2011, **50**, 6601-6608.

7. H. Yue, Y. Zhao, L. Zhao, J. Lv, S. Wang, J. Gong and X. Ma, *Aiche Journal*, 2012, **58**, 2798-2809.
8. Pruettt and R. L., *Science*, 1981, **211**, 11-16.
9. A. Yin, C. Wen, X. Guo, W.-L. Dai and K. Fan, *Journal of Catalysis*, 2011, **280**, 77-88.
10. C. Wen, Y. Cui, W.-L. Dai, S. Xie and K. Fan, *Chemical Communications*, 2013, **49**, 5195-5197.
11. P. Ai, M. Tan, N. Yamane, G. Liu, R. Fan, G. Yang, Y. Yoneyama, R. Yang and N. Tsubaki, *Chemistry - A European Journal*, 2017, **23**.
12. X. H, J. Z, J. L, Y. H, Y. P, J. R, *New Journal of Chemistry*, 2019, **43**.
13. C. Liang, G. Sha and S. Guo, *Journal of Non-Crystalline Solids*, 2000, **271**, 167-170.
14. F. J. Maldonado-Hódar, J. Rivera-Utrilla and C. Moreno-Castilla, *Carbon*, 1999, **37**, 1199-1205.
15. C. Moreno-Castilla and F. J. Maldonado-Hódar, *Carbon*, 2005, **43**, 455-465.
16. R. Saliger, U. Fischer, C. Herta and J. Fricke, *Journal of Non-Crystalline Solids*, 1998, **225**, 81-85.
17. D. Wu, R. Fu, S. Zhang, M. S. Dresselhaus and G. Dresselhaus, *Carbon*, 2004, **42**, 2033-2039.
18. Z. Guo, H. Zhu and X. Zhang, *Journal of Beijing Jiaotong University*, 2010, **34**, 103-106.
19. F. Tuinstra and J. L. Koenig, *Journal of Chemical Physics*, 1970, **53**, 1126-1130.
20. K. Nakamura, *Carbon*, 1998, **36**, 1693-1696.
21. Z. Wang, Z. Lu, X. Huang, R. Xue and L. Chen, *Carbon*, 1998, **36**, 51-59.
22. A. Yin, X. Guo, W.-L. Dai and K. Fan, *J.phys.chem.c*, 2009, **113**, 11003-11013.
23. P. Ai, M. Tan, Y. Ishikuro, Y. Hosoi, G. Yang, Y. Yoneyama and N. Tsubaki, *Chemcatchem*, 2017, **9**, 307--315.
24. D. Wang, G. Yang, Q. Ma, M. Wu, Y. Tan, Y. Yoneyama and N. Tsubaki, *Acs Catalysis*, 2012, **2**, 1958-1966.
25. M. Enterría, M. F. R. Pereira, J. I. Martins and J. L. Figueiredo, *Carbon*, 2015, **95**, 72-83.
26. H. Zhe, H. Lin, H. Ping and Y. Yuan, *Journal of Catalysis*, 2011, **277**, 54-63.
27. H. Zhang, Y. A. Alhamed, W. Chu, Z. Ye, A. AlZahrani and L. Petrov, *Applied Catalysis A General*, 2013, **464**, 156-164.
28. H. Zhang, C. Lancelot, W. Chu, J. P. Hong, A. Y. Khodakov, P. A. Chernavskii, J. Zheng and D. G. Tong, *J. Mater. Chem.*, 2009, **19**, 9241-9249.
29. L. He, X. Li, W. Lin, W. Li, H. Cheng, Y. Yu, S.-i. Fujita, M. Arai and F. Zhao, *Journal of Molecular Catalysis A Chemical*, 2014, **392**, 143-149.
30. A. Yin, X. Guo, W.-L. Dai, H. Li and K. Fan, *Applied Catalysis A General*, 2008, **349**, 91-99.
31. A. Yin, X. Guo, K. Fan and W. L. Dai, *Applied Catalysis A General*, 2010, **377**, 128-133.
32. Y. Zhao, S. Li, Y. Wang, B. Shan, J. Zhang, S. Wang and X. Ma, *Chemical Engineering Journal*, 2017, **313**, 759-768.
33. E. K. Poels and D. S. Brands, *Applied Catalysis A General*, 2010, **31**, no-no.
34. S. G. Popa, B. S. Ungureanu, I. A. Gheonea, A. Mitrea and A. Săftoiu, *Rom J Morphol Embryol*, 2015, **56**, 1495-1502.
35. B. Lin, K. Wei, J. Ni and J. Lin, *Chemcatchem*, **5**, 1941-1947.
36. K. Sun, W. Lu, F. Qiu, S. Liu and X. Xu, 2003, **252**, 243-249.
37. H. Ying, H. Ariga, X. Zheng, X. Duan and Y. Yuan, *Journal of Catalysis*, 2013, **307**, 74-83.

Graphical Abstract



The modification of B in carbon support can modulate the hydrogenation selectivity.